PHYSICAL REVIEW APPLIED **15,** 054065 (2021)

All-optical Helicity-Independent Switching State Diagram in Gd-Fe-Co Alloys

Jiaqi Wei,[1,2,‡] Boyu Zhang,[1,2,‡] Michel Hehn,[2] Wei Zhang,[2] Gregory Malinowski,[2] Yong Xu,[1]
Weisheng Zhao,[1,*] and Stéphane Mangin[2,†]

[1] *Fert Beijing Institute, Beijing Advanced Innovation Center for Big Data and Brain Computing (BDBC), School of Integrated Circuit Science and Engineering, Beihang University, Beijing 100191, China*
[2] *Université de Lorraine, CNRS, IJL, F-54000 Nancy, France*

(Received 28 January 2021; accepted 16 April 2021; published 28 May 2021)

Ultrafast magnetization switching induced by a single femtosecond laser pulse, under no applied magnetic field has attracted a lot of attention in the last 10 years because of its high potential for low-energy and ultrafast memory applications. Single-pulse helicity-independent switching has mostly been demonstrated for Gd-based materials. It is now necessary to optimize the pulse duration and the energy needed to switch a Gd-Fe-Co magnet depending on the alloy thickness and composition. Here we experimentally report state diagrams showing the magnetic state obtained after one single pulse depending on the laser pulse duration and fluence for various Gd-Fe-Co thin films with different compositions and thicknesses. We demonstrate that these state diagrams share similar characteristics: the fluence window for switching narrows for longer pulse duration and for the considered pulse-duration range the critical fluence for single-pulse switching increases linearly as a function of the pulse duration while the critical fluence required for creating a multidomain state remains almost constant. Calculations based on the atomistic spin model qualitatively reproduce the experimental state diagrams and their evolution. By studying the effect of the composition and the thickness on the state diagram, we demonstrate that the best energy efficiency and the longest pulse duration for switching are obtained for composition around the magnetic compensation.

DOI: 10.1103/PhysRevApplied.15.054065

I. INTRODUCTION

The rapidly increasing social needs for digital information drive the development of magnetic recording technology. In magnetic memory devices, digital information is stored by setting the magnetization of storage medium either "up" or "down." The data writing speed is therefore determined by how fast the setting process could be achieved [1–3]. The conventional way to switch the magnetization is by applying a magnetic field, which normally requires high power consumption and complex circuit design [4,5]. Later, various methods for manipulating the magnetization without the magnetic field emerged continuously, including strain [6,7], electric field [8,9], heat [10,11], and polarized current [12,13]. However, the switching process in above cases usually happens via a coherent damping precession of the spins [14,15]. The frequency of the precession is normally in the GHz range and the reorientation process can take several nanoseconds [16,17]. Therefore, a faster writing method is increasingly pursued by researchers.

Concerning the effect of ultrashort light pulse on magnetization, the field opened in 1996 with the discovery of ultrafast demagnetization of a Ni film by a 60-fs optical laser pulse [18]. A decade later, Stanciu *et al.* [19] demonstrated the possibility of using circular femtosecond laser pulses to induce ultrafast magnetization switching in Gd-Fe-Co, namely all-optical switching (AOS), which not only removes the need for magnetic field but also drives writing time towards the picosecond timescale. Soon after, it was discovered that a single linearly polarized pulse is sufficient to switch the Gd-Fe-Co, which is called all-optical helicity-independent switching (AO HIS) [20,21].

The mechanism behind AO HIS in Gd-Fe-Co alloys has been explained by the presence of two magnetization sublattices with two different relaxation times leading to a transient ferromagneticlike state [20]. Later, Gorchon *et al.* studied the role of electron and phonon temperatures in AO HIS [22]. According to these works, the laser fluence should be high enough to sufficiently heat the free electrons, and initiate the demagnetization and switching process. On the other hand, the laser fluence should also ensure that the phonon temperature T_{ph} remains below T_C, since crossing T_C would lead to magnetic disorder and the final magnetization state would then be determined by the

---

[*] weisheng.zhao@buaa.edu.cn
[†] stephane.mangin@univ-lorraine.fr
[‡] These authors contributed equally to this work.

cooling conditions. Therefore, AO HIS should occur only within a narrow range of pulse fluence. In addition, the pulse duration is another useful laser parameter. As mentioned above, high T_e is essential for AOS, so it is predicted that the maximum pulse duration ($\tau_{\max}$) should be on the timescale of the electron-lattice interaction τ_{e-l} (around 2 ps in Gd-Fe-Co [23]) in order to reach an overheating of the electrons. However, AOS with a pulse duration up to 15 ps was reported [22]. Moreover, two recent works on AO HIS in Gd-Fe-Co have demonstrated that $\tau_{\max}$ is significantly influenced by the Gd concentration [23,24].

Despite several works investigating the effect of single-shot AO HIS, the influence of the laser parameters such as fluence and pulse duration and the properties of the Gd-Fe-Co sample such as the concentration and the thickness, has not been systematically investigated. In this work, we report the AO HIS state diagrams for Gd-Fe-Co thin films for different compositions and thicknesses by determining the magnetic configuration as a function of laser-pulse duration and fluence. These state diagrams allow us to identify the ideal material and beam parameters to obtain an energy-efficient switching. We also define the critical switching fluence (F^{C}_{switch}) as the minimum fluence allowing the switching of a given alloy thin film. It is usually obtained for the shortest pulse duration. We demonstrate that F^{C}_{switch} reaches a minimum around the magnetization compensation point. The state diagram is also significantly influenced by the sample thickness. A thinner film allows the maximum pulse duration necessary to be increased to achieve AO HIS. These findings on the influence of the laser parameters and thin-film properties on AO HIS allow a better understanding of the fundamental mechanism behind this switching.

II. RESULTS

A. Sample structure and characterization

We prepare a series of 10- and 20-nm-thick $\mathrm{Gd}_x(\mathrm{FeCo})_{100-x}$ layers with different Gd concentrations ranging from 22 to 27%. The amorphous alloys are ferrimagnetic metallic materials, with two antiferromagnetically exchange-coupled sublattices. The net magnetization of the alloy is given by the sum of the transition metal (FeCo) sublattice magnetization and the rare-earth (Gd) sublattice magnetization. Therefore, by tuning the composition of the $\mathrm{Gd}_x(\mathrm{FeCo})_{100-x}$, it is possible to modulate the magnetic properties. For a composition called the magnetization compensation point ($x = x_{\text{comp}}$), the net magnetization reaches zero and the coercivity diverges.

The investigated samples are deposited by dc magnetron sputtering onto a glass substrate according to the following multilayered structure: glass/Ta (3 nm)/Pt (5 nm)/$\mathrm{Gd}_x(\mathrm{FeCo})_{100-x}$ (t nm)/Ta (5 nm). The thin Ta capping layer on top prevents the oxidation of the magnetic film, while it allows probing of the magnetic properties via magneto-optical Kerr effect (MOKE). The bottom Ta layer improves adhesion of the structure to the glass substrate. According to the magnetic hysteresis loops obtained by MOKE, all studied samples show strong perpendicular magnetic anisotropy (PMA). From the MOKE results, at room temperature, we could determine x_{comp} between 24% and 25% (MOKE results are provided in Note S1 within the Supplemental Material [25]). The net magnetic moment is thus aligned in the direction of the FeCo magnetization sublattice below x_{comp} while it changes its sign and becomes aligned with the Gd magnetization sublattice above x_{comp}. Note that x_{comp} also depends on the temperature.

B. Magnetization state diagram of Gd-Fe-Co

Figure 1(a) shows magneto-optical images obtained on a 20-nm $\mathrm{Gd}_{24}(\mathrm{FeCo})_{76}$ film after exposure to a single laser pulse for different pulse durations (50 fs, 1 ps, and 3 ps) and different fluences. The film is initially saturated under an external magnetic field before exposure. We observe that above a certain fluence defined as F_{switch}, the magnetization of the Gd-Fe-Co switches (evidences of AO HIS for the studied samples are supplied in Note S2 within the Supplemental Material [25]). Moreover, the spot showing AO HIS expands as the fluence increases and a similar trend is shown for different pulse durations. It is clear that F_{switch} depends on the pulse duration. For fluences lower than F_{switch} the laser has no effect on the magnetic configuration (not shown). Above a given fluence F_{multi}, multiple domains start to appear in the middle of the spot. Consequently, AO HIS is only observed for a fluence value between F_{switch} and F_{multi}. In addition, as displayed in Fig. 1(b), fully demagnetized patterns are only found when the pulse duration increases to 4 ps, indicating that deterministic all-optical switching could not be achieved above certain pulse duration whatever the laser fluence. Note that the AO HIS state diagram is very different from that of all-optical helicity-dependent switching (AO HDS) such as the one obtained by Kichin *et al.* [26]. Indeed, for AO HIS the fluence window for switching narrows as the pulse duration increases, which is opposite to the trend observed for AO HDS for which the fluence window broadens as the pulse duration increases. This is one more proof that the mechanism behind the two types of switching (AO HIS and AO HDS) are different [27].

To gain a more detailed insight of the dependence of AO HIS on the pulse characteristics, F_{switch} and F_{multi} are presented as a function of the pulse duration indicated by full blue squares and full red dots, respectively, as shown in Fig. 1(c). The open black squares indicate the F_{switch} obtained via the method proposed by Liu *et al.* [28]. A full description of this technique is supplied in Note S2 within the Supplemental Material [25]. This AO HIS

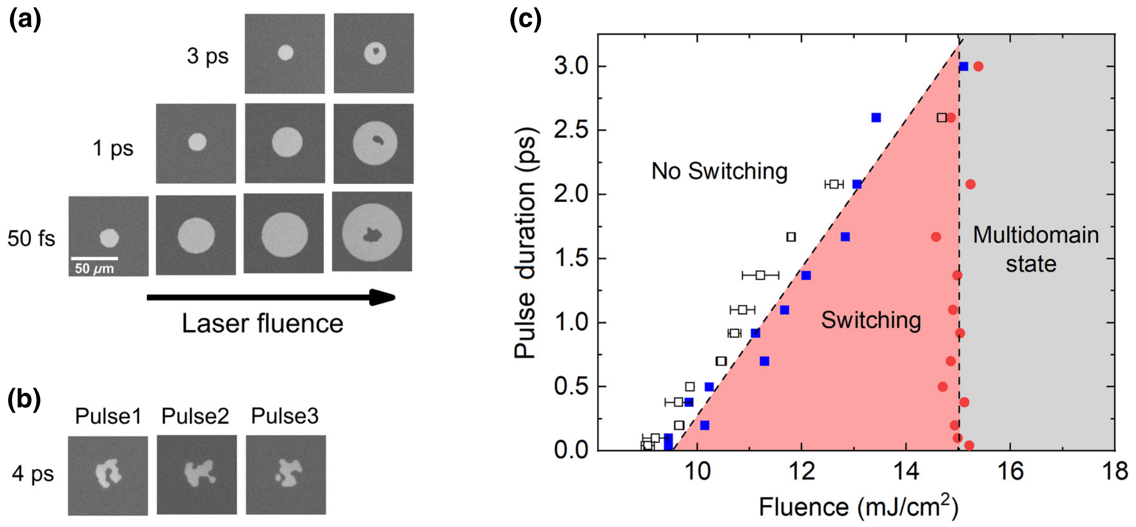

FIG. 1. Magneto-optical images and all-optical helicity-independent switching state diagram for a 20-nm $Gd_{24}(FeCo)_{76}$ film. (a) Magneto-optical images of $Gd_{24}(FeCo)_{76}$ after exposure to a single linearly polarized laser pulse with a pulse duration of 50 fs, 1 ps, and 3 ps, and with various fluences ranging from 9.5 to 15 mJ/cm^2. (b) Magneto-optical images of $Gd_{24}(FeCo)_{76}$ after exposure to a single linearly polarized laser pulse with a pulse duration of 4 ps and a fluence of 17 mJ/cm^2. (c) AO HIS state diagram: switching fluence F_{switch} (open black square and full blue square) and multidomain fluence F_{multi} (full red dot) as a function of the pulse duration for a single linearly polarized laser pulse. The blue full squares represent the switching fluences F_{switch} recorded when the diameter of switched area reaches around 10 μm. The open squares are the fitting results obtained via the method proposed by Liu *et al.* [28]. The spatial FWMH of laser beam is around 70 μm.

state diagram allows defining the single-pulse laser characteristics leading to AO HIS, multidomain state or no reversal. Moreover, F_{switch} and F_{multi} show obviously different dependences on pulse duration. F_{multi} is independent on the pulse duration in this pulse-duration range, whereas F_{switch} shows in first approximation a linear increase as the pulse duration increases until $F_{\text{switch}}{=}F_{\text{multi}}$, which defines the maximum pulse duration ($\tau_{\max}$) for which AO HIS can be observed. Increasing further the pulse duration leads only to a multidomain state.

C. AO HIS state diagrams as a function of the Gd concentration

Figures 2(a) and 2(b) present AO HIS state diagrams for 20-nm $Gd_x(FeCo)_{100-x}$ films, with $22 \leq x \leq 27$ [see Fig. S7 within the Supplemental Material for state diagrams [25] in 10-nm $Gd_x(FeCo)_{100-x}$]. One can see that the switching regions for different samples share similar outlines (highlighted by colored dashed lines). Indeed, for all concentrations, F_{switch} increases linearly with the pulse duration and F_{multi} is independent of the pulse duration. However, obvious changes can be found as the composition is varied. For a more quantitative analysis, the switching region in the state diagram can be characterized by a right triangle. It is mathematically determined by the smallest switching fluence F^C_{switch} (the x-axis intercept of linear fit of F_{switch}), F_{multi}, and the slope k describing the dependence of F_{switch} on pulse duration. It is seen that F^C_{switch} shows a minimum around 25% Gd concentration, which is near the magnetization compensation point x_{comp}. The slope k increases with the Gd concentration while F_{multi} decreases, which can be attributed to the reduction of the Curie temperature with the Gd composition [24]. We then observe that the fluence range showing AO HIS is larger and the maximum pulse duration ($\tau_{\max}$) is longer around x_{comp}. A complete AOS is observed for laser pulse durations up to 3.8 ps for $Gd_{25}(FeCo)_{75}$. This contradicts the trend predicted by Davis *et al.* that $\tau_{\max}$ linearly increases with the Gd concentration [23]. Figure 3 quantitatively shows F^C_{switch} and k as a function of the Gd concentration derived from the AO HIS state diagrams. It is seen that F^C_{switch} and k share similar trends in 10- and 20-nm samples. However, F^C_{switch} scales with the layer thickness as shown in Fig. 3(a); a larger k is obtained for 10-nm Gd-Fe-Co at a fixed composition as shown in Fig. 3(b). As a consequence, a complete AO HIS is observed in 10-nm $Gd_{25}(FeCo)_{75}$ for a pulse duration up to 11.8 ps, which is consistent with the observation of AO HIS for a 14-nm Gd-Fe-Co layer and a pulse duration around 10 ps [22]. The state diagrams for 10-nm samples are provided in Note S3 within the Supplemental Material [25].

D. Atomistic modeling for single-shot AO HIS

In this section, our goal is to test if atomistic modeling can reproduce the experimental results shown above. In the atomistic calculations, each spin is coupled to the

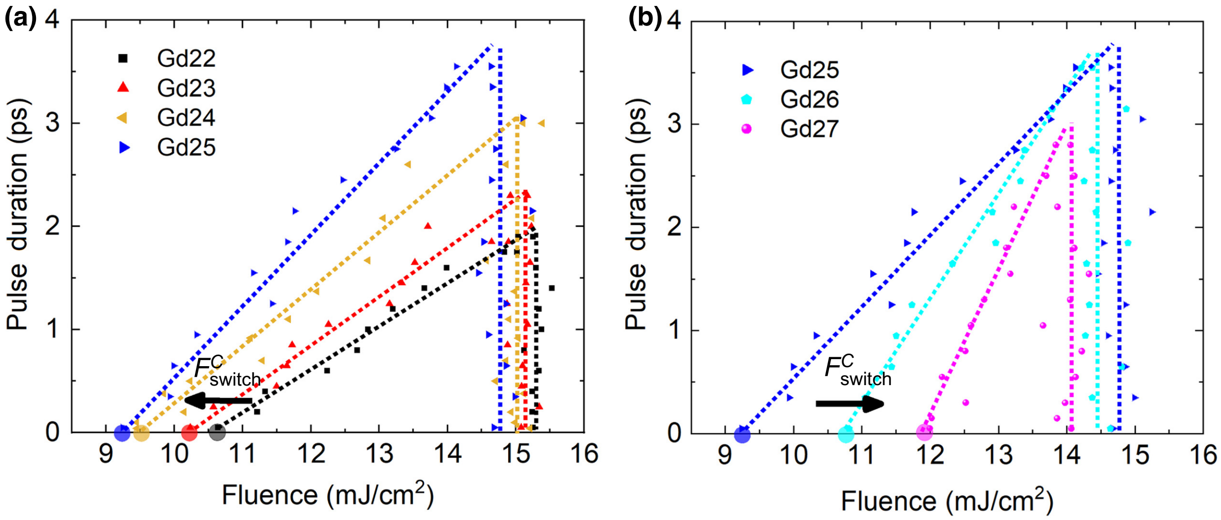

FIG. 2. AO HIS state diagrams of 20 nm $\mathrm{Gd}_x(\mathrm{FeCo})_{100-x}$ for (a) $22 \le x \le 25$ and (b) $25 \le x \le 27$. The switching regions for different Gd concentrations are highlighted by colored dashed lines. They are mathematically determined by the smallest switching fluence F^C_{switch} (the x-axis intercept of linear fit of F_{switch}), F_{multi} and the slope k describing the dependence of F_{switch} on pulse duration.

temperature of the electron thermal bath. Due to the small heat capacity of electrons, the action of the ultrashort laser pulse first induces a rapid increase of the electron temperature, followed by a slow heat exchange between the electron and phonon thermal baths until equilibrium is reached. The temporal evolution of the electron temperature T_e and the phonon temperature T_{ph} are described by the two-temperature model described in Ref. [29]. To simplify calculations, Fe and Co are considered as one sublattice and share the same parameters taken from Refs. [30–32]. Simulations are performed using the VAMPIRE software package [33].

We then simulate the temporal evolution of magnetization of Gd and FeCo to an ultrafast light pulse (see Note S4 within the Supplemental Material [25]). Here, we determine the magnetization state after laser excitation according to the value of the z component of FeCo magnetization $m_z^{\mathrm{FeCo}}(t)$ when $t = 20$ ps: (1) switching $[m_z^{\mathrm{FeCo}}(20) \le -0.1]$, (2) multidomain $[-0.1 < m_z^{\mathrm{FeCo}}(20) < 0.1]$, (3) no switching $[m_z^{\mathrm{FeCo}}(20) \ge 0.1]$. We choose "20 ps" to allow for magnetization recovery. Based on such a definition, we obtain the simulated state diagram as shown in Fig. 4. It is seen that F_{switch} greatly increases from 5.16 mJ/cm^2 at 50 fs to 7.92 mJ/cm^2 at 1 ps while only a little change could

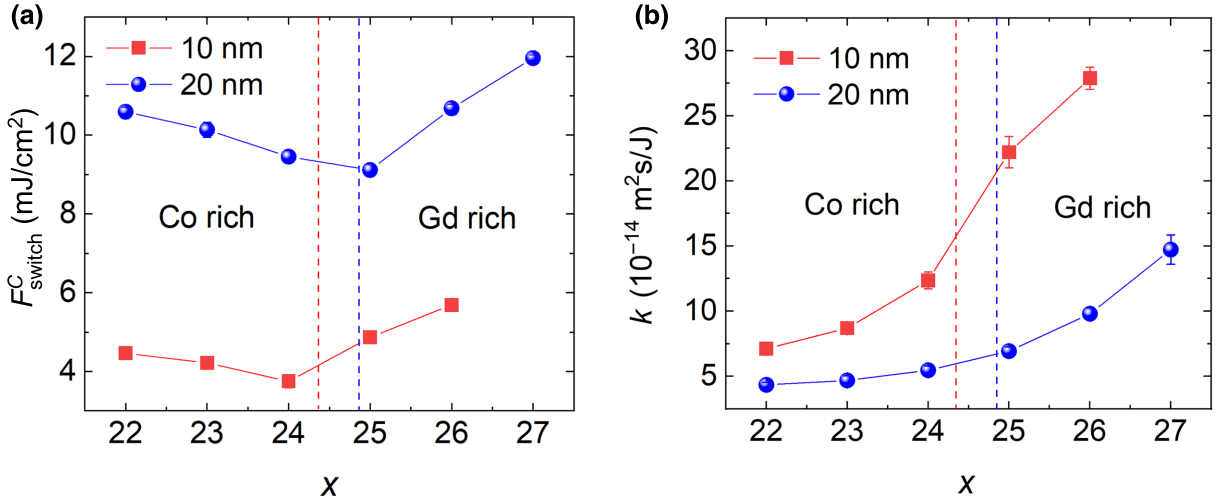

FIG. 3. Quantitative description of the key features of AO HIS $\mathrm{Gd}_x(\mathrm{FeCo})_{100-x}$ state diagrams. (a) The critical switching fluence F^C_{switch} obtained from the intercept of linear fit of F_{switch} on the x axis is plotted as a function of Gd concentration. (b) Evolution of the slope k extracted from the linear fit of F_{switch} as a function of Gd concentration.

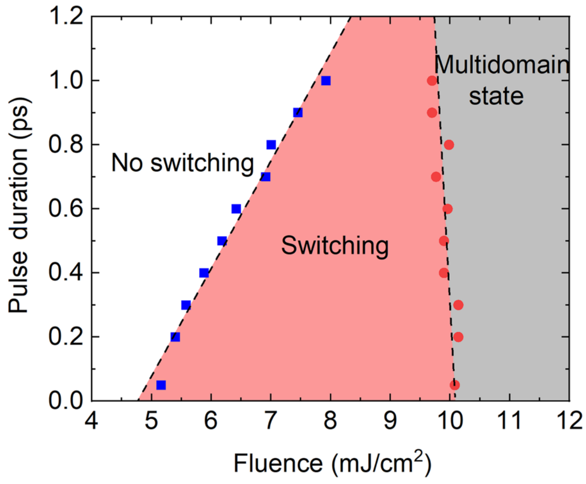

FIG. 4. Simulated state diagram for $Gd_{26}(FeCo)_{74}$. Blue squares and red dots indicate F_{switch} and F_{multi}, respectively. Dashed lines show linear fits.

be observed in F_{multi}, which agrees well with the experimental state diagram. As the pulse broadens, the increase in F_{switch} is necessary for achieving an overheating of the free electrons, which seems to be crucial for AO HIS. In addition, we calculate the temporal evolution of phonon temperature T_{ph} at F_{multi} for different pulse durations (see Note S4 within the Supplemental Material [25]). Interestingly, the peak T_{ph} shows almost no change for different pulse durations. As a consequence, it depends mostly on the pulse energy and reaches T_c at a very similar fluence for different pulse durations.

Then we try to plot k for different Gd concentrations. As shown in Fig. 5(a), we calculate F_{switch} for several pulse durations and compositions. The slope k derived from the linear fit shows a monotonically increase with Gd concentration as presented in Fig. 5(b). This indicates that when the pulse duration increases by a certain amount, the rise in F_{switch} required to induce AO HIS is smaller for the samples with more Gd. This is likely because that the laser heating has a more significant effect with the increased Gd content due to the reduction in Curie temperature T_C. Lastly, we calculate F_{switch} as a function of Gd concentration for 50-fs pulse duration. As displayed in Fig. 5(c), F_{switch} depends significantly on the Gd concentration, and reaches a minimum around 32% Gd. This trend is quite similar to the one observed in the experiments. However, the calculated x_{comp} is around 26 (see Note S4 within the Supplemental Material [25]), which differs from the composition where the minimum F_{switch} is obtained. This shift could be explained by a very recent work, which shows the position of the F_{switch} minimum with respect to the Gd-concentration varies with the ratio $\alpha_{\mathrm{Fe}}/\alpha_{\mathrm{Gd}}$ utilized in the atomistic modeling [24].

III. DISCUSSION

The experimental AO HIS state diagrams allow to quickly visualize the laser-pulse conditions (fluence and pulse duration) required for single-shot AO HIS. We can then determine the evolution of the state diagrams as a function of the Gd-Fe-Co alloy concentration and thickness. This experimental study helps to address technologically relevant controversy and provides crucial guidelines to engineer energy-efficient and technologically feasible single-pulse all-optical switching of magnetization (a detailed discussion is provided in Note S5 within the Supplemental Material [25]). Since it has already been shown that both single femtosecond light pulse and single femtosecond hot electron pulse [34] can induce AO HIS, the next issue is to generalize the effect to longer pulses to be technologically compatible with feasible electronics. Our study allows answering two controversial questions: how can we optimize the material and the laser excitation to obtain a low-energy AO HIS and how can we observe AO HIS for long pulse duration?

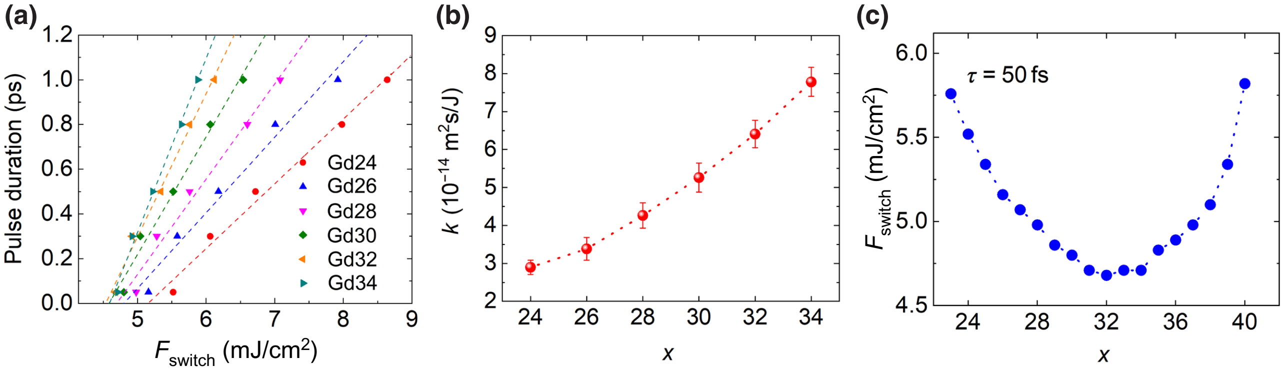

FIG. 5. Quantitative description of the key features of simulated AO HIS $Gd_x(FeCo)_{100-x}$ state diagrams. (a) Simulated slopes describing the dependence of F_{switch} on pulse duration for different Gd concentrations. Dashed lines are the linear fits. (b) Slope k as a function of Gd concentration derived from the data shown in (a). (c) F_{switch} as a function of Gd concentration for a pulse duration of 50 fs.

For the first question, initial studies proposed that the existence of magnetization compensation temperature T_M is essential to achieve AO HIS in ferrimagnets [35]. Later, it was proved that T_M is not indispensable while low net magnetization M_{net} greatly promotes AO HIS [36]. However, a following theory work highlighted the relevance of temperature derivative of the magnetization $dM_{\text{net}}(T)/dT$ and it pointed out that the critical switching fluence is not the minimum at magnetization compensation point x_{comp} [37]. In our study, we experimentally demonstrate that F^C_{switch} significantly depends on the alloy composition and reaches a minimum around x_{comp}. We also find that F^C_{switch} scales with the layer thickness, which can be ascribed to the variation of the laser absorption and the domain volume, indicating that a smaller thickness helps to develop energy-efficient AOS devices (more results are provided in Note S6 within the Supplemental Material [25]).

The second issue concerns the pulse-duration threshold $\tau_{\max}$. As mentioned above, previous works highlight the relevance of dramatic overheating of electrons. Therefore, it is initially predicted that $\tau_{\max}$ should be at the timescale of the electron-lattice interaction τ_{e-l} (around 2 ps in Gd-Fe-Co). However, further studies have shown disparate results ranging from 0.4 to 15 ps [22,23], which could appear surprising at first. In our work, we reveal that $\tau_{\max}$ is determined by F^C_{switch}, which defines the base of the triangle-shaped switching region and the slope k, which describes the dependence of F_{switch} on pulse duration and F_{multi}, which seems to be given by the material Curie temperature. To obtain the largest $\tau_{\max}$ we should just aim for a small F^C_{switch}, a large F_{multi} and a large k. However, k increases with Gd concentration whereas F_{multi} decreases with Gd concentration and F^C_{switch} is minimum around the magnetic compensation alloy composition. Therefore, to maximize $\tau_{\max}$ it is certainly interesting to be close to the compensation to obtain the smallest F^C_{switch}, but it is also interesting to play with the relative Fe and Co concentration in order to increase the alloys' Curie temperature and increase k. In addition, a recent work on AO HIS in Gd-Tb-Co highlights that the damping of the rare earth site has an obvious influence on F_{switch} [38]. Thus we propose that the magnetization state diagram could also be modified by adding different elements, which will be a subject of future work. The influence of the sample thickness on AO HIS is more complicated than it appears. From the state diagrams, the right triangle-shaped switching region for 10-nm Gd-Fe-Co possesses a much steeper slope than that for 20-nm Gd-Fe-Co, which results in a larger $\tau_{\max}$. This difference is likely caused by the nonuniform light absorption with respect to the sample depth. Xu *et al.* have calculated the heat-absorption profile for similar 20-nm Gd-Fe-Co stacks [27]. They revealed that the electron temperature sharply decreases within the bottom 5-nm part of a 20-nm Gd-Fe-Co film when excited with a laser having a wavelength of 800 nm. Therefore, it needs much more energy to induce an overheating for thicker samples as pulse duration increases, leading to a smaller k.

IV. CONCLUSION

In conclusion, precise single-shot AO HIS state diagrams for various $\text{Gd}_x(\text{FeCo})_{100-x}$ are built. It is found that the critical fluences for AO HIS and multidomain state exhibit different pulse-duration dependences. Calculations based on atomistic spin model are able to reproduce the behaviors observed experimentally. This reveals that electron temperature and lattice temperature play useful roles in the all-optical magnetization switching. In addition, we demonstrate that the dependence of the critical switching fluence on pulse duration can be tuned by changing the alloy composition and thickness. These results provide a way to enlarge the switching region of AO HIS, which will be of great significance for the application of AO HIS since the present semiconductor laser sources can only generate laser pulses with picosecond temporal width [39] where the fluence window for AO HIS is extremely narrow or even vanishes and the switching fluence is much larger than that for femtosecond laser pulse.

ACKNOWLEDGMENTS

This work is supported by the ANR-15-CE24-0009 UMAMI and the ANR-20-CE09-0013, by the Institute Carnot ICEEL for the project "Optic-switch" and Matelas, by the Région Grand Est, by the Metropole Grand Nancy, by the impact project LUE-N4S, part of the French PIA project "Lorraine Université d'Excellence," reference ANR-15-IDEX-04-LUE, and by the "FEDER-FSE Lorraine et Massif Vosges 2014-2020," a European Union Program. The authors gratefully acknowledge the National Natural Science Foundation of China (Grant No. 61627813), the Program of Introducing Talents of Discipline to Universities (Grant No. B16001) and the Beijing Municipal Science and Technology Project (Grant No. Z201100004220002).

[1] J. Hu, Z. Li, L. Chen, and C. Nan, High-density magnetoresistive random access memory operating at ultralow voltage at room temperature, Nat. Commun. **2**, 553 (2011).

[2] A. D. Kent and D. C. Worledge, A new spin on magnetic memories, Nat. Nanotechnol. **10**, 187 (2015).

[3] K. C. Chun, H. Zhao, J. D. Harms, T. Kim, J. Wang, and C. H. Kim, A scaling roadmap and performance evaluation of in-plane and perpendicular MTJ based STT-MRAMs for high-density cache memory, IEEE J. Solid-State Circuits **48**, 598 (2013).

[4] B. N. Engel, J. Åkerman, B. Butcher, R. W. Dave, M. DeHerrera, M. Durlam, G. Grynkewich, J. Janesky, S. V. Pietambaram, N. D. Rizzo, J. M. Slaughter, K. Smith, J. J. Sun, and S. Tehrani, A 4-Mb toggle MRAM based on

a novel Bit and switching method, IEEE Trans. Magn. **41,** 132 (2005).

[5] X. Xiang, T. Zhu, F. Sheng, Z. Zhang, and J. Xiao, Recent developments in magnetic tunnel junctions, IEEE Trans. Magn. **39,** 2770 (2003).

[6] F. Motti, G. Vinai, A. Petrov, B. A. Davidson, B. Gobaut, A. Filippetti, G. Rossi, G. Panaccione, and P. Torelli, Strain-induced magnetization control in an oxide multiferroic heterostructure, Phys. Rev. B **97,** 094423 (2018).

[7] O. Kovalenko, T. Pezeril, and V. V. Temnov, New Concept for Magnetization Switching by Ultrafast Acoustic Pulses, Phys. Rev. Lett. **110,** 266602 (2013).

[8] S. H. Chun, Y. S. Chai, B. Jeon, H. J. Kim, Y. S. Oh, I. Kim, H. Kim, B. J. Jeon, S. Y. Haam, J. Park, S. H. Lee, J. Chung, J. Park, and K. H. Kim, Electric Field Control of Nonvolatile Four-State Magnetization at Room Temperature, Phys. Rev. Lett. **108,** 177201 (2012).

[9] R. O. Cherifi, V. Ivanovskaya, L. C. Phillips, A. Zobelli, I. C. Infante, E. Jacquet, V. Garcia, S. Fusil, P. R. Briddon, N. Guiblin, A. Mougin, A. A. Ünal, F. Kronast, S. Valencia, B. Dkhil, A. Barthélémy, and M. Bibes, Electric-field control of magnetic order above room temperature, Nat. Mater. **13,** 345 (2014).

[10] Z. Li and S. Zhang, Thermally assisted magnetization reversal in the presence of a spin-transfer torque, Phys. Rev. B **69,** 134416 (2004).

[11] S. Wienholdt, D. Hinzke, K. Carva, P. M. Oppeneer, and U. Nowak, Orbital-resolved spin model for thermal magnetization switching in rare-earth-based ferrimagnets, Phys. Rev. B **88,** 020406 (2013).

[12] S. Mangin, D. Ravelosona, J. A. Katine, and E. E. Fullerton, Current-induced magnetization reversal in nanopillars with perpendicular anisotropy, Nat. Mater. **5,** 210 (2006).

[13] M. Wang, W. Cai, K. Cao, J. Zhou, J. Wrona, S. Peng, H. Yang, J. Wei, W. Kang, Y. Zhang, J. Langer, B. Ocker, A. Fert, and W. Zhao, Current-induced magnetization switching in atom-thick tungsten engineered perpendicular magnetic tunnel junctions with large tunnel magnetoresistance, Nature Commun. **9,** 671 (2018).

[14] L. D. Landau and E. M. Lifshitz, On the theory of the dispersion of magnetic permeability in ferromagnetic bodies, Phys. Z. Sowjetunion **8**, 153 (1935).

[15] T. L. Gilbert, A Lagrangian formulation of the gyromagnetic equation of the magnetization field, Phys. Rev. **100**, 1243 (1955).

[16] A. Kamra, R. E. Troncoso, W. Belzig, and A. Brataas, Gilbert damping phenomenology for two-sublattice magnets, Phys. Rev. B **98,** 184402 (2018).

[17] T. Weindler, H. G. Bauer, R. Islinger, B. Boehm, J. Chauleau, and C. H. Back, Magnetic Damping: Domain Wall Dynamics Versus Local Ferromagnetic Resonance, Phys. Rev. Lett. **113,** 237204 (2014).

[18] E. Beaurepaire, J. Merle, A. Daunois, and J. Bigot, Ultrafast Spin Dynamics in Ferromagnetic Nickel, Phys. Rev. Lett. **76,** 4250 (1996).

[19] C. D. Stanciu, F. Hansteen, A. V. Kimel, A. Kirilyuk, A. Tsukamoto, A. Itoh, and T. Rasing, All-Optical Magnetic Recording with Circularly Polarized Light, Phys. Rev. Lett. **99,** 047601 (2007).

[20] I. Radu, K. Vahaplar, C. Stamm, T. Kachel, N. Pontius, H. A. Dürr, T. A. Ostler, J. Barker, R. F. L. Evans, R. W. Chantrell, A. Tsukamoto, A. Itoh, A. Kirilyuk, T. Rasing, and A. V. Kimel, Transient ferromagnetic-like state mediating ultrafast reversal of antiferromagnetically coupled spins, Nature **472,** 205 (2011).

[21] T. A. Ostler, et al., Ultrafast heating as a sufficient stimulus for magnetization reversal in a ferrimagnet, Nat. Commun. **3,** 666 (2012).

[22] J. Gorchon, R. B. Wilson, Y. Yang, A. Pattabi, J. Y. Chen, L. He, J. P. Wang, M. Li, and J. Bokor, Role of electron and phonon temperatures in the helicity-independent all-optical switching of GdFeCo, Phys. Rev. B **94,** 184406 (2016).

[23] C. S. Davies, T. Janssen, J. H. Mentink, A. Tsukamoto, A. V. Kimel, A. F. G. van der Meer, A. Stupakiewicz, and A. Kirilyuk, Pathways for Single-Shot All-Optical Switching of Magnetization in Ferrimagnets, Phys. Rev. Appl. **13,** 024064 (2020).

[24] F. Jakobs, T. Ostler, C. Lambert, Y. Yang, S. Salahuddin, R. B. Wilson, J. Gorchon, J. Bokor, and U. Atxitia, Unifying femtosecond and picosecond single-pulse magnetic switching in GdFeCo, Preprint at https://arxiv.org/abs/2004.14844 (2020).

[25] See Supplemental Material at http://link.aps.org/supplemental/10.1103/PhysRevApplied.15.054065 for more detailed information about the experiments, the MOKE results of all the studied samples, a brief discussion of the atomistic modeling, and further experimental and numerical results supporting our conclusions.

[26] G. Kichin, M. Hehn, J. Gorchon, G. Malinowski, J. Hohlfeld, and S. Mangin, From Multiple- to Single-Pulse All-Optical Helicity-Dependent Switching in Ferromagnetic Co / Pt Multilayers, Phys. Rev. Appl. **12,** 024019 (2019).

[27] Y. Xu, M. Hehn, W. Zhao, X. Lin, G. Malinowski, and S. Mangin, From single to multiple pulse all-optical switching in GdFeCo thin films, Phys. Rev. B **100,** 064424 (2019).

[28] J. M. Liu, Simple technique for measurements of pulsed Gaussian-beam spot sizes, Opt. Lett. **7,** 196 (1982).

[29] S. I. Anisimov, B. L. Kapeliovich, and T. L. Perelman, Electron emission from metal surfaces exposed to ultrashort laser pulses, Zh. Eksp. Teor. Fiz. **66**, 375 (1974).

[30] R. F. L. Evans, W. J. Fan, P. Chureemart, T. A. Ostler, M. O. A. Ellis, and R. W. Chantrell, Atomistic spin model simulations of magnetic nanomaterials, J. Phys. Condens. Matter **26,** 103202 (2014).

[31] T. A. Ostler, R. F. L. Evans, R. W. Chantrell, U. Atxitia, O. Chubykalo-Fesenko, I. Radu, R. Abrudan, F. Radu, A. Tsukamoto, A. Itoh, A. Kirilyuk, T. Rasing, and A. Kimel, Crystallographically amorphous ferrimagnetic alloys: Comparing a localized atomistic spin model with experiments, Phys. Rev. B **84,** 024407 (2011).

[32] J. Barker, U. Atxitia, T. A. Ostler, O. Hovorka, O. Chubykalo-Fesenko, and R. W. Chantrell, Two-magnon bound state causes ultrafast thermally induced magnetisation switching, Sci. Rep. **3,** 03262 (2013).

[33] VAMPIRE software package. Available from https://vampire.york.ac.uk/.

[34] Y. Xu, M. Deb, G. Malinowski, M. Hehn, W. Zhao, and S. Mangin, Ultrafast magnetization manipulation using single femtosecond light and Hot-electron pulses, Adv. Mater. **29,** 1703474 (2017).

[35] C. D. Stanciu, A. Tsukamoto, A. V. Kimel, F. Hansteen, A. Kirilyuk, A. Itoh, and T. Rasing, Subpicosecond Magnetization Reversal Across Ferrimagnetic Compensation Points, Phys. Rev. Lett. **99**, 047601 (2007).

[36] A. Hassdenteufel, J. Schmidt, C. Schubert, B. Hebler, M. Helm, M. Albrecht, and R. Bratschitsch, Low-remanence criterion for helicity-dependent all-optical magnetic switching in ferrimagnets, Phys. Rev. B **91**, 104431 (2015).

[37] U. Atxitia, T. A. Ostler, R. W. Chantrell, and O. Chubykalo-Fesenko, Optimal electron, phonon, and magnetic characteristics for low energy thermally induced magnetization switching, Appl. Phys. Lett. **107**, 192402 (2015).

[38] A. Ceballos, A. Pattabi, A. El-Ghazaly, S. Ruta, C. P. Simon, R. F. L. Evans, T. Ostler, R. W. Chantrell, E. Kennedy, M. Scott, J. Bokor, and F. Hellman, Role of element-specific damping on the ultrafast, helicity-independent all-optical switching dynamics in amorphous (Gd, Tb)Co thin films, Preprint at https://arxiv.org/abs/1911.09803 (2019).

[39] B. Xu, H. Wang, Z. Cen, Z. Liu, K. Ye, H. Yang, J. Zhang, and J. Li, Simulation study of pulse laser quality effects on recording performances of heat-assisted magnetic recording by short-pulse laser heating, IEEE Trans. Magn. **51**, 3101905 (2015).